SAND REPORT
SAND2001-2898
Unlimited Release
Printed September 2001

Report on the Fracture Analysis of HfB_2-SiC and ZrB_2-SiC Composites

John J. Mecholsky, Jr.

Prepared by
Sandia National Laboratories
Albuquerque, New Mexico 87185 and Livermore, California 94550

Sandia is a multiprogram laboratory operated by Sandia Corporation, a Lockheed Martin Company, for the United States Department of Energy under Contract DE-AC04-94AL85000.

Sandia National Laboratories

Issued by Sandia National Laboratories, operated for the United States Department of Energy by Sandia Corporation.

Available to DOE and DOE contractors from
U.S. Department of Energy
Office of Scientific and Technical Information
P.O. Box 62
Oak Ridge, TN 37831

Telephone: (865)576-8401
Facsimile: (865)576-5728
E-Mail: reports@adonis.osti.gov
Online ordering: http://www.doe.gov/bridge

Available to the public from
U.S. Department of Commerce
National Technical Information Service
5285 Port Royal Rd
Springfield, VA 22161

Telephone: (800)553-6847
Facsimile: (703)605-6900
E-Mail: orders@ntis.fedworld.gov
Online order: http://www.ntis.gov/ordering.htm

SAND2001-2898
Unlimited Release
Printed October 2001

Report on the Fracture Analysis of HfB_2-SiC and ZrB_2-SiC Composites

John J. Mecholsky,Jr.
Advanced Materials Laboratory
Sandia National Laboratories
P. O. Box 5800
Albuquerque NM 87185-1349

Abstract

Hafnium diboride-silicon carbide (HS) and zirconium diboride-silicon carbide (ZS) composites are potential materials for high temperature, thermal shock applications such as for components on re-entry vehicles. In order to establish material constants necessary for evaluation of *in situ* fracture, bars fractured in four-point flexure were examined using fractographic principles. The fracture toughness was determined from measurements of the critical crack sizes and the strength values and the crack branching constants were established to use in forensic fractography for future in-flight tests. The fracture toughnesses range from about 13 $MPam^{1/2}$ at room temperature to about 6 $MPam^{1/2}$ at 1400°C for ZrB_2-SiC composites and from about 13 $MPam^{1/2}$ at room temperature to about 4 $MPam^{1/2}$ at 1400°C for HfB_2-SiC composites. Thus, the toughnesses of either the HS or ZS composites have the potential for use in thermal shock applications. Processing and manufacturing defects limited the strength of the test bars. However, examination of the microstructure on the fracture surfaces shows that the processing of these composites can be improved. There is potential for high toughness composites with high strength to be used in thermal shock conditions if the processing and handling are controlled.

Introduction

Hafnium diboride-silicon carbide (HS) and zirconium diboride-silicon carbide (ZS) composites are potential materials for high temperature, thermal shock applications such as for components on re-entry vehicles. In order to evaluate the properties of the materials to assess their applicability and to provide baseline data for future failure analysis, test bars were fabricated, machined and tested in four-point flexure to determine strength, elastic modulus, deflection and density by Southern Research Institute (SoRI). Some of the test bars were made available for further fractographic analysis by NASA Ames Research Center. Four billets of hafnium diboride-silicon carbide designated HS-04, HS-05, HS06 and HS07 and one billet of zirconium diboride-silicon carbide designated ZS-08 were made available. The fracture toughness in terms of the critical stress intensity factor was determined from the size of the fracture-originating crack at four temperatures: 21°C, 400°C, 1200°C and 1400°C. In addition, there was also limited, but useful, data on the boundaries of fracture mirrors surrounding the fracture initiating flaw. These measurements provided the baseline information necessary for future forensic analysis of *in situ* test results. The crack branching stress intensities were determined for several billets of the hafnium diboride and for one billet of the zirconium diboride. The purpose of this report is to evaluate the potential for use of these materials in a high-temperature, thermal shock environment and to suggest methods for improvement, if necessary.

Methodology

The fracture toughness of a material that fails in a brittle manner can be expressed by the critical stress intensity factor, K_{Ic}, a development of linear elastic fracture mechanics, LEFM. In an elastic material the stress field near a crack tip, as described by the stress intensity factor, K_I, is material independent, but depends on the geometry of the sample and the distance from the crack tip (1). The critical value of K_I, denoted K_{Ic}, is determined by:(2,3)

$$K_{Ic} = \alpha \sigma_f (\pi c)^{1/2} / \phi \qquad (1)$$

where α = surface correction and loading factor

σ_f = stress at fracture

c = crack size (equivalent semi-circular radius)

ϕ = crack geometry factor (elliptical integral of the second kind)

The elliptical integral accounts for the variation in the stress field due to the shape of the crack tip. For a semi-circular crack the value is $\pi/2$. For a surface crack that is small relative to the thickness, $\alpha \approx 1.10$. Any elliptical or semi-elliptical crack can be modeled as a semi-circular crack using $c = (ab)^{1/2}$, where 2a and 2b are the lengths of the minor and major axes of the elliptical crack, respectively.(4) The calculation of K_{Ic} assumes

that the material is linear elastic, that any surface effects are accounted for in the determination of α, and that the loading is tensile. Notice that if all flaws are made to have the size of their semi-circular equivalent, then Equation (1) becomes:

$$K_{Ic} = Y\sigma_f (c)^{1/2} \qquad (2)$$

where Y = 1.24 for a semi-circular crack that is small relative to the thickness, Y = 1.4 for a corner crack and Y = 2 for an internal crack. Minor modifications to standard LEFM theory can be made to account for a small zone of plasticity near the crack tip (3). The resulting equation is:

$$K_{Ic}^2 = (\alpha^2 \pi \sigma_f^2 c)/(\phi^2 - (0.212\sigma_f^2/\sigma_{ys}^2) \qquad (3)$$

where the terms are as previously defined and σ_{ys} = yield stress.

The topographic features of a fracture surface depend on the nature of the failure that created the surface.(5, 6) A schematic of a typical fracture surface is shown in Figure 1. The presence of the mirror region and the increase in roughness away from the flaw are characteristic of brittle fracture, although the appearance of the individual regions and the clarity of the boundaries between them may be altered due to microstructural features or anisotropy of the fractured material.(6). The flaw size and stress can be independently measured and used in equations 1 and 2 to determine the fracture toughness. This technique was developed for inorganic glasses (7) and used in the analysis of many other materials (8).

We observe that from the point of fracture, the crack propagates in a relatively smooth plane, called the mirror region, to the boundary, r_1. From this point the tortuosity discontinuously increases and the deviations from the plane progressively increase in a region known as mist, to the boundary r_2. At this point, there is another sharp increase in deviations out of plane in the region known as hackle. At the end of the hackle region, r_3, macroscopic crack branching occurs, i.e., the entire crack front branches as opposed to parts of the crack front branching as it does in the mirror, mist and hackle regions. Normally, we refer to the mirror-mist boundary, mist – hackle boundary and the macroscopic crack branching boundary. However, for ease of discussion, I shall refer to all of the boundaries as mirror boundaries and distinguish them by their r_j designation, where j = 1,2 or 3 depending on the boundary. These regions are all related to the applied (far field) stress at fracture, σ_f,:

$$K_{Bj} = Y\sigma_f (r_j)^{1/2}$$

or (4)

$$\sigma_f (r_j)^{1/2} = \frac{K_{Bj}}{Y'(\theta)} = M_j$$

where the M_j's are called mirror constants with j=1 corresponding to the mirror-mist boundary, etc., $Y'(\theta)$ is a crack border correction factor, where θ is the angle from the surface to the interior, i.e., $\theta = 0°$ to 90°. K_{Bj} is the notation for the crack branching stress intensity factors. There are three, one for each boundary, i.e., j=1, j=2 and j=3. Note that K_{Bj} is proportional to K_C, i.e., $K_{Bj} = \lambda K_C$, where λ is about 2-4 for most ceramic materials.

Results and Discussion

The fracture surfaces of flexure bars for HS-04, HS-05, HS-06, HS-07 and ZS-08 at four temperatures (21°C,400°C,1200°C & 1400°C) were examined to determine the size of the fracture initiating defect and the measurement of the surrounding topography, if available. An example of the appearance of the fracture surfaces with the crack outlined is shown in Figure 2. The tables containing the individual measurements and results of the calculations are included in an appendix to this report. The graphs of the fracture toughness as a function of temperature for HS-04, HS-05, HS-06, HS-07 and ZS-08 are included as Figures 3-7. Several of the bars showed an unusual fracture pattern to indicate that there may have been a misalignment during fracture. In addition, some of the bars had secondary breaks. This often happens if there is an uneven loading of the four-point flexure apparatus, i.e., one side of the top loading pins is loaded more than another side. The result of this uneven loading is that the stress at failure is not the same as the calculated maximum stress. Thus, because of these possible errors in loading, there may be a larger amount of scatter than usually encountered in fractographic analysis. However, the general behavior is correct.

In examining the graphs in Figures 3-7, several noteworthy points are observed. The potential fracture toughness of both the HS series and the ZS material is reasonably good for a brittle material, i.e., at room temperature the ZS-08 has an average toughness of 13 ± 3 MPa $m^{1/2}$ and HS-07 also has an average toughness of 13 ± 3 MPa $m^{1/2}$. It appears that the toughness is also greater at 400°C. The reason for this increase is not known at this time, but the increase has been observed for all of the billets except one. The strength data also show this increase at 400°C for most of the materials measured. The strength as a function of temperature for representative materials, i.e., HS-04, HS-07 and ZS-08, are presented in Figures 8-10. In addition, the elastic moduli (E), which were measured by SoRI, show a similar trend as a function of temperature [Figures 11-15] in that the moduli stay about the same or increase for the HS composites at room temperature and 400°C. The only anomaly is that the moduli appear to decrease monotonically as a function of temperature for ZS-08. The toughness values should be proportional to the elastic modulus if these materials behave as most ceramic materials. The graph of K_C versus E are shown in Figures 16-20. As can be seen within the scatter of the data, there is a linear relationship between toughness and modulus for these materials.

One of the other observations is that there are billet-to-billet differences in fracture behavior. This indicates that better control in processing is needed. Also, notice

that the toughness values are reduced considerably at high temperatures, i.e., at 1200°C and 1400°C. The fractographic analysis showed that there was some slow crack growth at these temperatures, e.g., Figure 21. The original cracks were comparable in size to the size of cracks leading to failure at 21°C and 400°C. But at the higher temperatures, the cracks grew from this initial size to a much larger size. This can be noted in the tables in the appendix by comparing average crack sizes at the different temperatures. The high temperature crack growth can partly explain the low strength values at the high temperatures. However, this cannot be the cause of the low toughness values and thus cannot explain the entire strength decrease. There has to be a change in the microstructural integrity at high temperatures to decrease the toughness.

There were only a few bars on which the surrounding crack topography could be determined. However, there were enough measurements that a reasonable estimate of the crack branching stress intensities can be made. The results of this analysis are shown in Table 1. The mirror constants are given, along with the corresponding crack branching stress intensities. The supporting measurements are provided in the appendix. The values of the crack branching stress intensities can be used to estimate the stress at fracture from measurements of the mirror boundaries in the same material. It has been shown that the stress at fracture can be reasonably estimated even when the stress field is complex. This is because the fracture of materials that fail in a brittle manner, fail when the crack is approximately perpendicular to the maximum principal tensile stress and the critical stress intensity level is reached.

As a check on the fractographic approach to stress analysis, Figures 22-24 are graphs of the branching stress intensities, K_{B1}, K_{B2} and K_{B3}, respectively, versus the fracture toughness, K_C. There should be a constant relationship between these values and as can be seen, there is a reasonable agreement. The branching constant values that are provided in the tables are estimates based on all of the bars that were examined. For future studies, care should be taken to insure wide enough samples to gather as much data as possible.

Application of Fracture Analysis To Future In-flight Test Results

Materials on re-entry vehicles will be subjected to high temperatures for a relatively short time. This exposures means that the materials must be able to withstand thermal shock environments. The constants determined in this report are essential for future flight test result analysis. The value of toughness that is needed for calculation of thermal shock resistance is the toughness at or near room temperature. Even though the initial temperature may be large, the thermal shock response will take place in a matter of seconds or not at all, because thermal shock fracture is a result of transient thermal stresses. Fracture from thermal shock must be distinguished from fracture at high temperatures. Thermal stresses developed in thermal shock are delivered in a relatively short period of time and the location of the large tensile stresses are away from the heated region. In fact, many times the thermal stresses are developed on the surface during cool down, which is also rapid. Thus, the material properties of importance are those near room temperature even though some parts of the specimens are at high temperatures.

Fracture from high temperature exposure can involve some high temperature process before fracture, such as slow crack growth or creep before catastrophic fracture. These processes are usually relatively slow and need time for reactions to occur. Although the high temperature behavior here is important for overall understanding of the microstructure-property relationship, it is less important for the understanding of thermal shock behavior.

In the future, thermal shock tests should be performed in order to assess the mechanical response to this type of stimulus. For example, quench tests into oil or water are a possibility. Water is not as good as oil because of the difficulty in knowing the heat transfer coefficient for quenching into water. If a continuous-wave laser with at least capability of 1 kw/cm^2, and a spot size of at least 1 cm^2, is available, then irradiation of a thin, i.e., < 1 cm, plate of the material can be a quick test of the thermal shock resistance of the materials.

Conclusions and Recommendations

1. The toughnesses of ZrB_2-SiC and HfB_2-SiC composites are sufficient for use in a thermal shock environment.
2. Processing and manufacturing defects limited the strength of the bars.
3. Processing of the materials can be improved.
4. Fractographic principles can be used in future failure analysis of *in situ* tests of components from these materials.
5. Wider test bars should be fabricated in any future flexure tests in order to be able to measure the mirror boundaries and obtain the necessary constants for forensic analysis.
6. Careful attention should be given to the alignment and rotational flexibility of any four-point flexure test set-up to avoid errors in loading.
7. Thermal shock tests such as quenching in water or oil or CW laser irradiation should be planned to evaluate the thermal shock capabilities.

References

1. G. W. Irwin, Trans, ASME, J. Appl. Mech., **24**, 361 (1957).
2. G. W. Irwin, Trans. ASME, J. Appl. Mech., **29**, 651 (1962).
3. P. N. Randall, in Plain Strain Crack Toughness Testing of High Strength Metallic Materials, ASTM STP 410,W. F. Brown, Jr. and J. E. Swraley, Eds., American Society for Testing and Materials, West Conshohocken, PA, 1967, pp. 88-126.
4. J. J. Mecholsky, S. W. Freiman and R. W. Rice, J. Am. Ceram. Soc., **60**, 114 (1977).
5. Mecholsky, J. J., Jr., "Quantitative Fractography: An Assessment." In: Ceramic Transactions, Vol. 17, *Fractography of Glasses and Ceramics I.* Frechette VD, Varner J, editors. Westerville: American Ceramic Society, 1991,pp. 413-451.
6. American Society of Testing and Materials Standard C1322-96a, Fractographic Analysis. ASTM, Warrendale, PA. 1996

7. J. J. Mecholsky Jr., in Experimental Techniques of Glass Science C. J. Simmons, O. H. El-Bayoumi, Eds., American Ceramic Society, Columbus, OH, 1993, pp.483-520.
7. J. J. Mecholsky Jr., in Fractography of Glasses and Ceramics III J. P. Varner, V. D. Frechette, G. D. Quinn, Eds., American Ceramics Society, Columbus, OH, 1996, pp. 385-393.

Table 1 -	Crack branching Data										
Designation	Strength (ksi)	Strength(MPa)	r_1	r_2	r_3	M_1	M_2	M_3	K_{B1}	K_{B2}	K_{B3}
			m 10^6	m 10^6	m 10^6	MPam$^{1/2}$	MPam$^{1/2}$	MPam$^{1/2}$	MPam$^{1/2}$	MPam$^{1/2}$	MPam$^{1/2}$
ZS08-1 (21C)	79	545	690	1020	1700	14.3	17.4	22.5	17.7	21.6	27.9
ZS08-13 (21C)	77.6	535	550	900	1340	12.5	16.1	19.6	15.5	20.0	24.3
						13.4	**16.8**	**21.1**	**16.6**	**20.8**	**26.1**
ZS08-14(400C)	89.4	616	1090	1900		20.3	26.9		25.2	33.4	
ZS08-18	86.2	594	1080	1550		19.5	23.4		24.2	29.0	
						19.9	**25.2**		**24.7**	**31.2**	
ZS08-22(1200C	37.9	261	1390			9.7			12.0		
ZS08-4(1400C)	46.3	319		870	2200		9.4	15.0	1.2	11.7	18.6
ZS08-8	36.9	254	1000	1150	3170	8.0	8.6	14.3	9.9	10.7	17.7
							9.0	**14.7**	**5.6**	**11.2**	**18.2**
HS04-9 (21C)	33	228	1260	2100		8.1	10.4		10.0	12.9	
HS04-13(21C)	41.5	286	770	1260	2100	7.9	10.2	13.1	9.8	12.6	16.3
HS04-17(21C)	39.2	270	600	1150	1700	6.6	9.2	11.1	8.2	11.4	13.8
						7.5	**9.9**	**12.1**	**9.3**	**12.3**	**15.1**
HS05-13(21C)	62.6	432	740	1230	1850	11.8	15.2	18.6	14.6	18.8	23

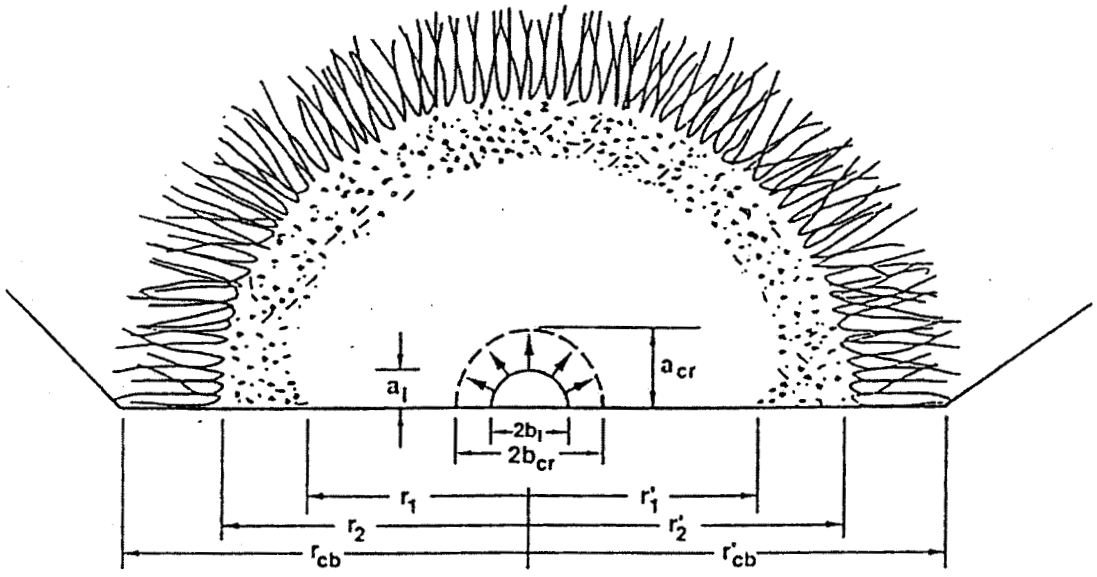

Figure 1 – Schematic of Fracture Surface. The critical crack size is $(a_{cr} \bullet b_{cr})^{1/2}$. r_1 is the distance to the mirror-mist boundary; r_2 is the distance to the mist-hackle boundary; and $r_{cb}(r_3)$is the distance to macroscopic crack branching. The difference between a_i, b_i and a_{cr} ,b_{cr}, is that there can be slow crack growth which increases the crack size before final fracture. The primes on the r_j's indicate that there can be asymmetrical boundaries.

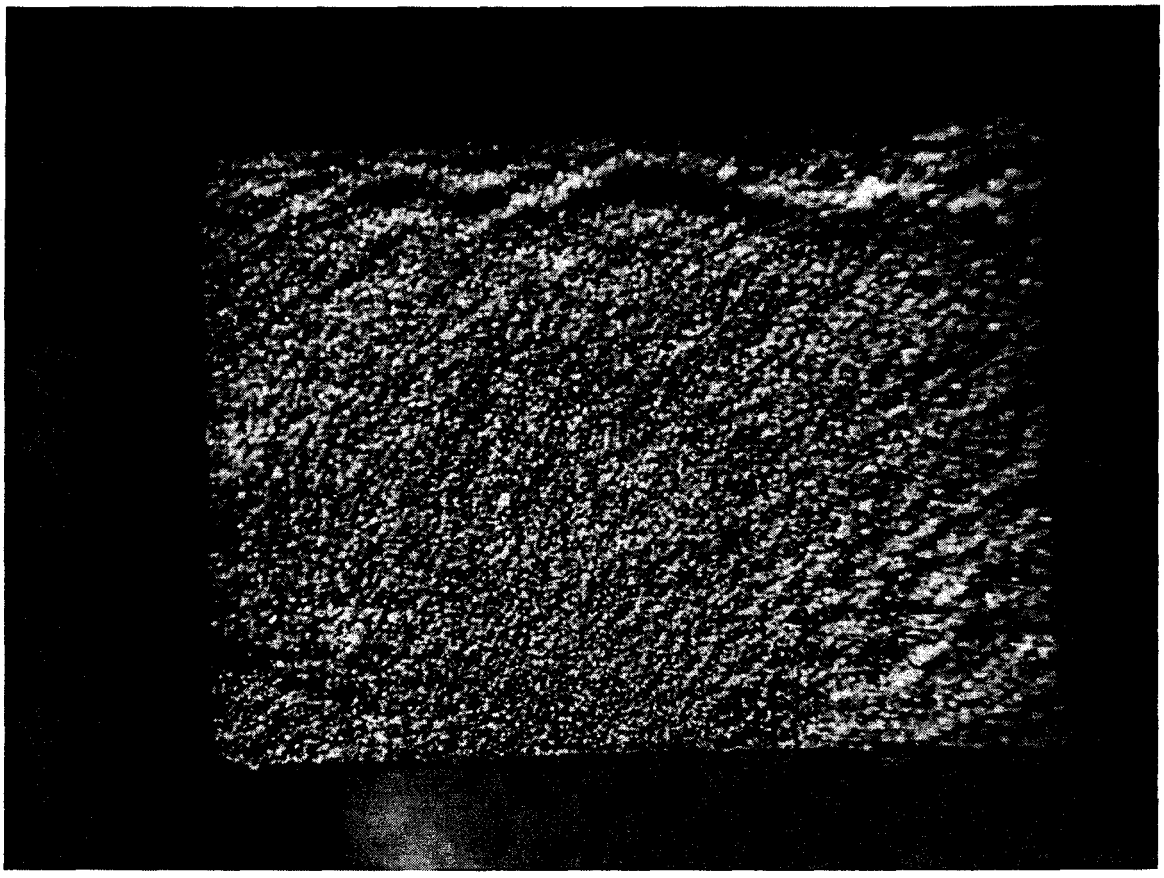

Figure 2A – Photograph of Fracture Surface of ZS-08 (#4) without markings. [1400°C/ 319 MPa]

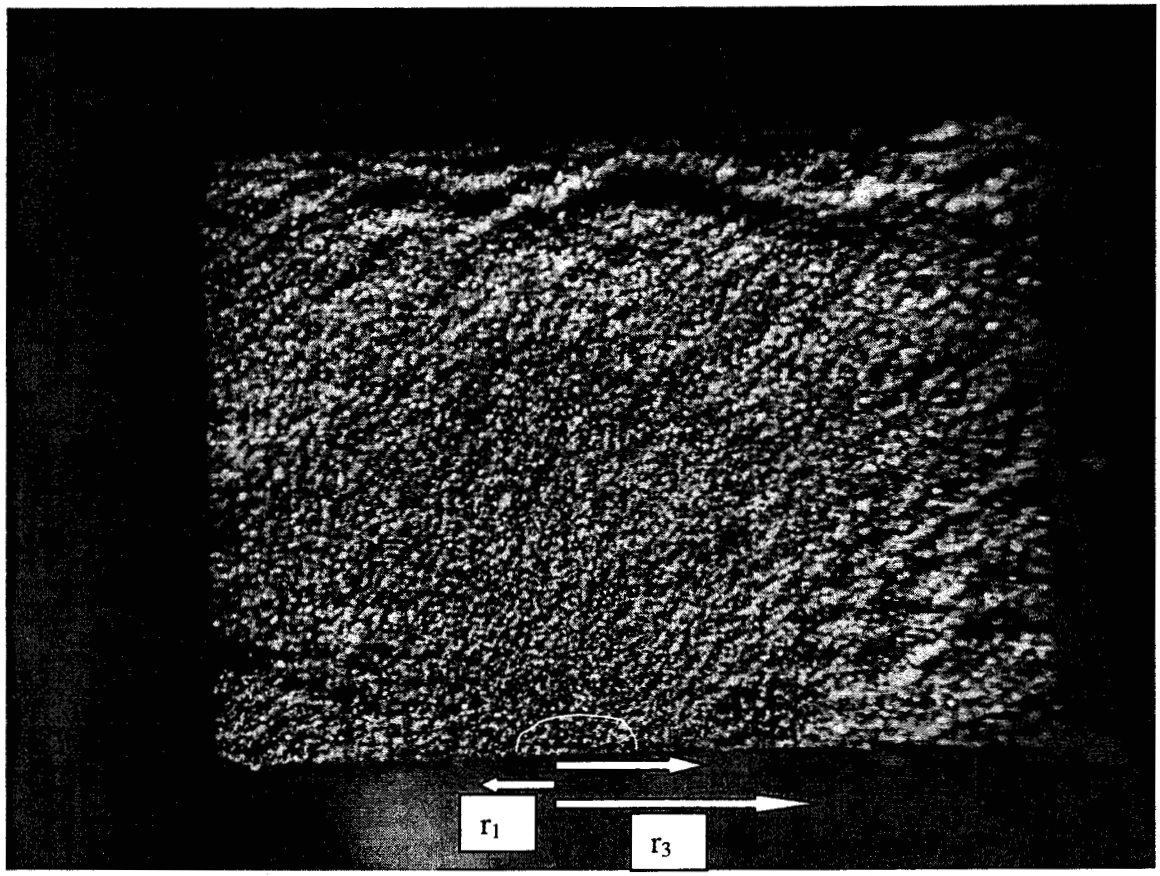

Figure 2B – Fracture Surface of ZS-08 (#4) Showing Regions Depicted in Figure 1. r_1 and r_3 are shown; r_2 is the unmarked arrow. The white line outlines the fracture initiating crack.

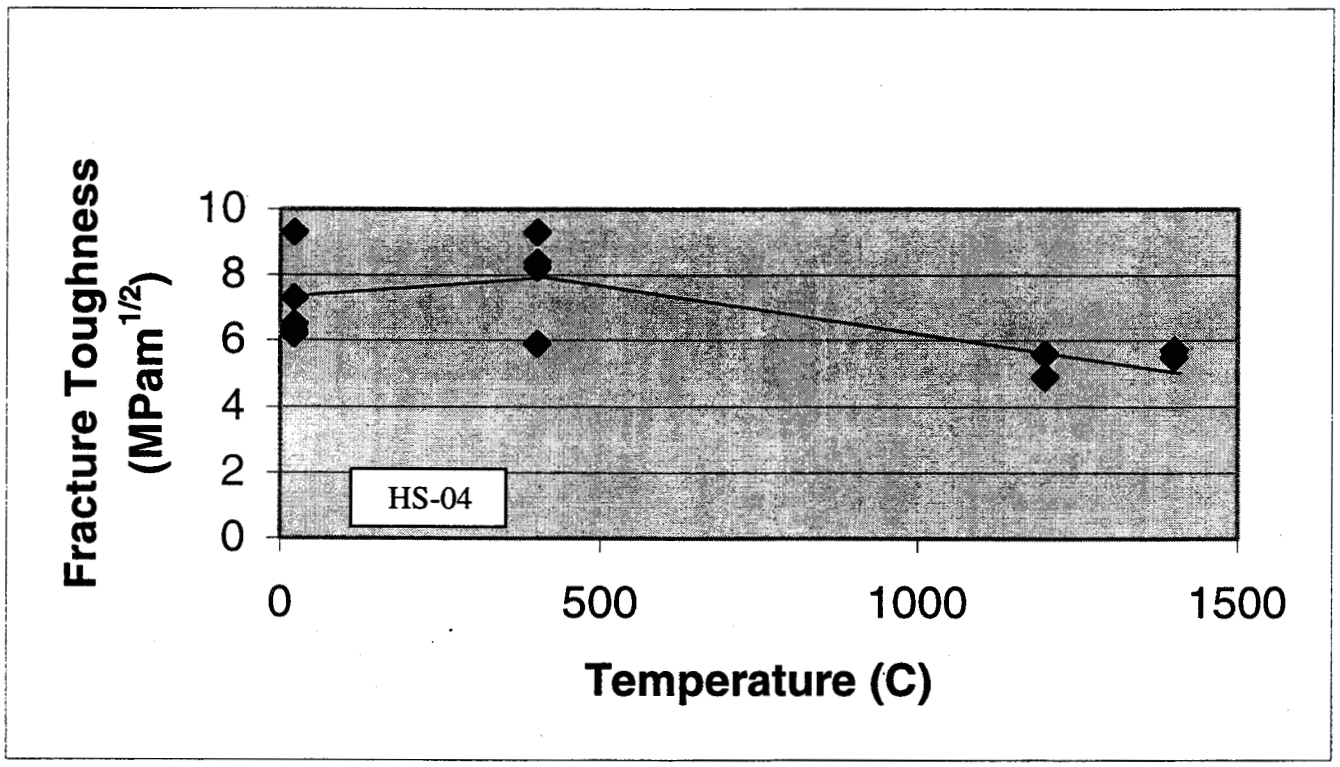

Figure 3 – Fracture Toughness As A Function of Temperature for HS-04.

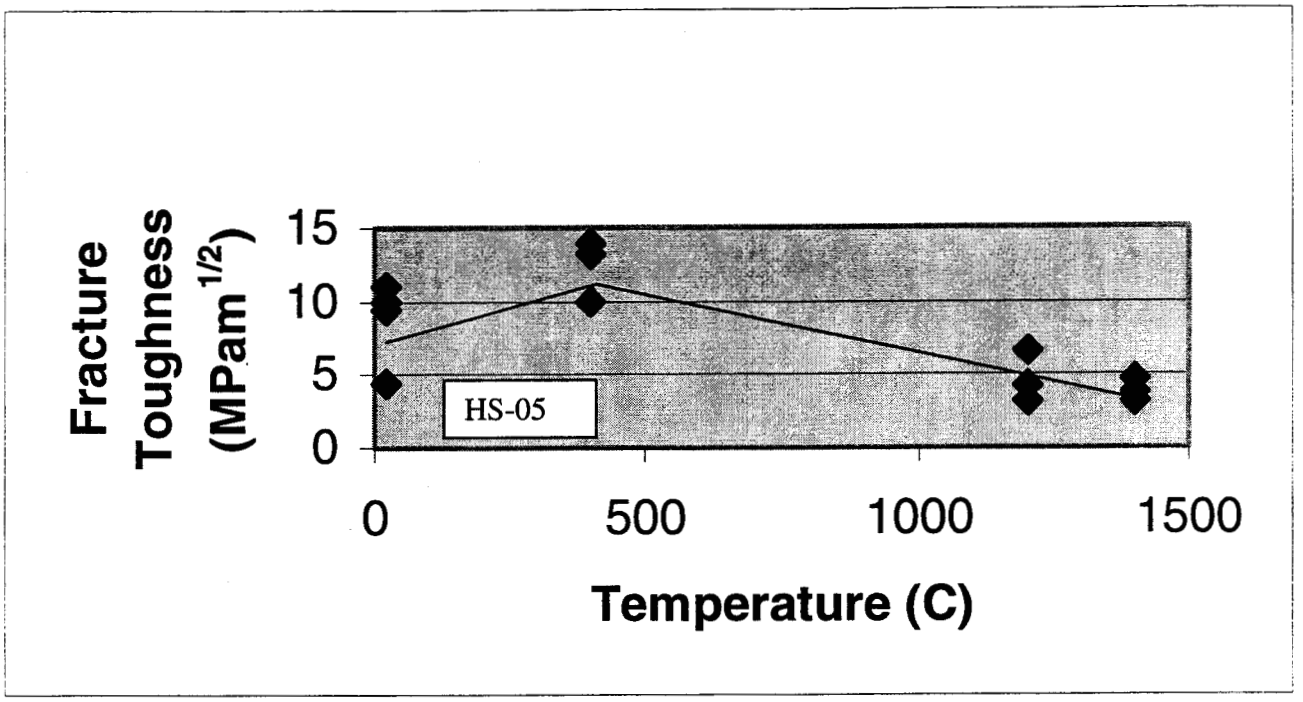

Figure 4 – Fracture Toughness Of HS-05 As A Function of Test Temperature.

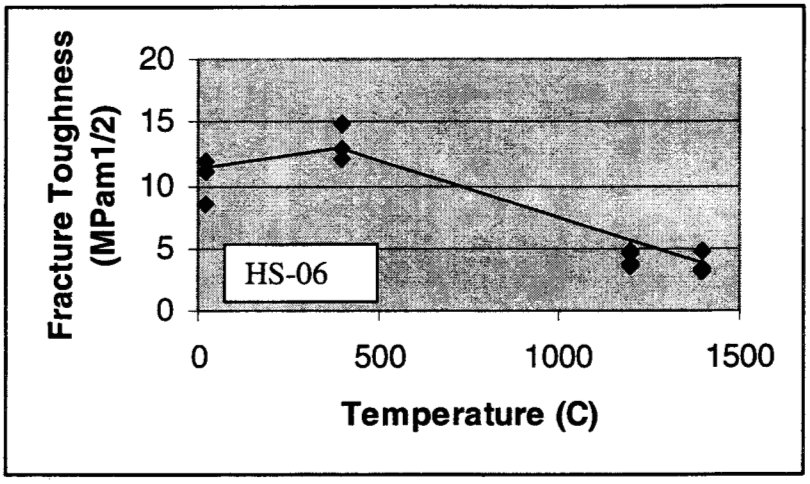

Figure 5- Fracture Toughness of HS-06 As A Function of Temperature.

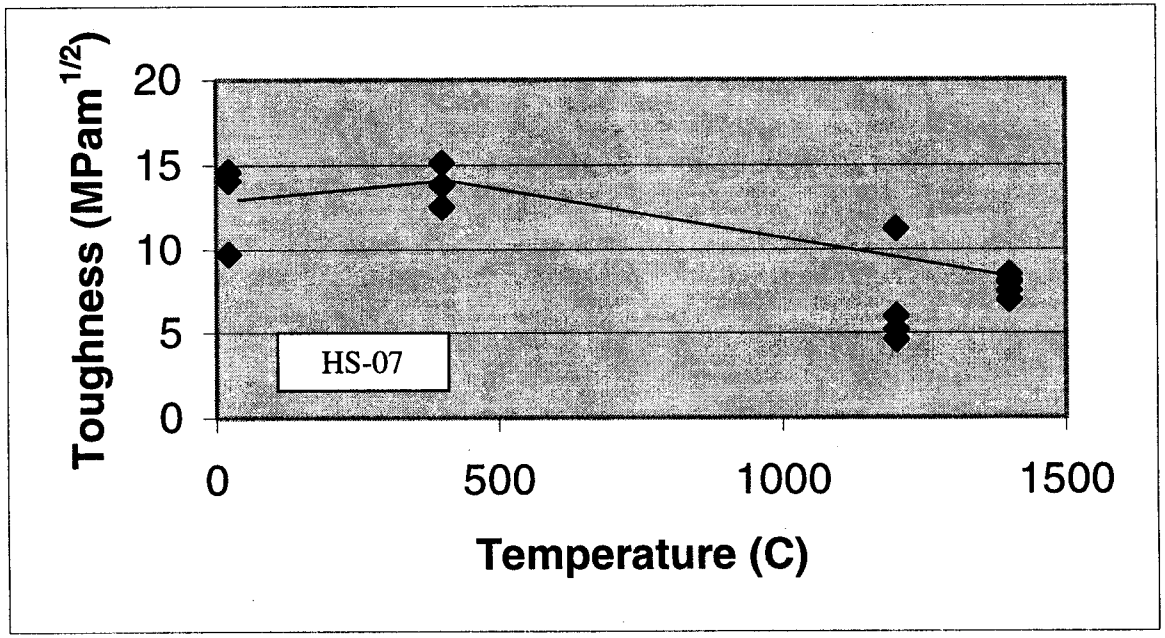

Figure 6- Fracture Toughness of HS-07 As A Function of Temperature

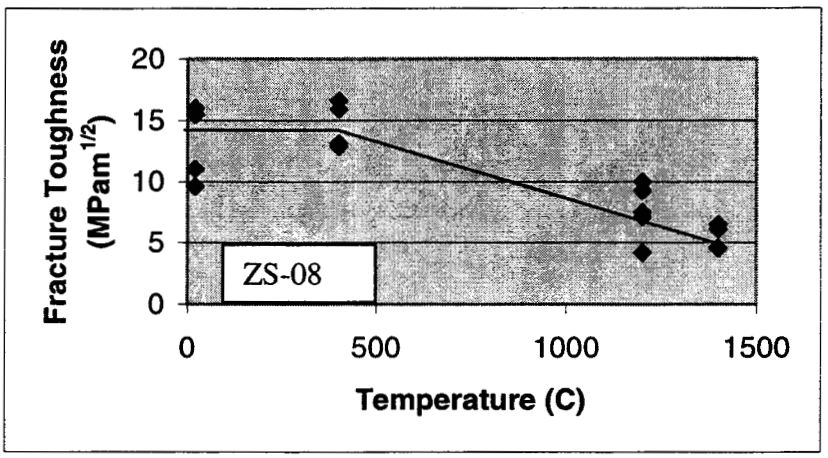

Figure 7 – Fracture Toughness of ZS-08 As A Function of Temperature

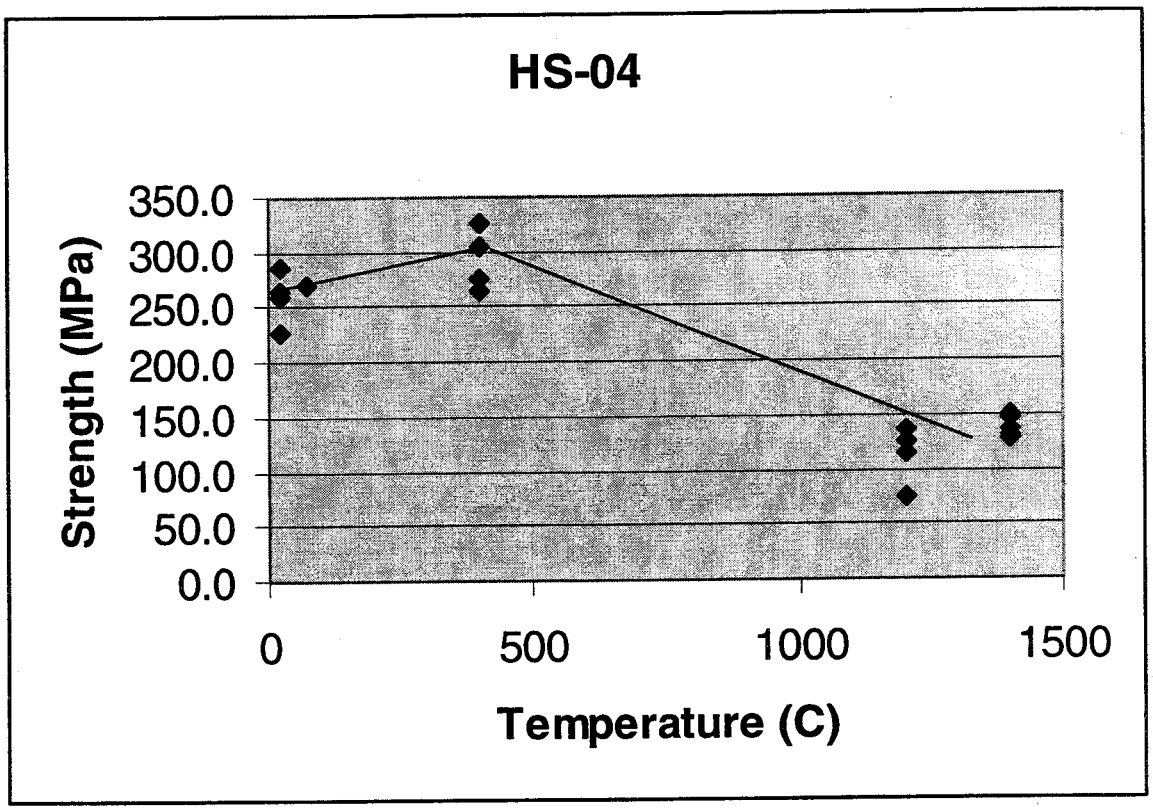

Figure 8 – Strength of Flexure Bars As A Function of Temperature.

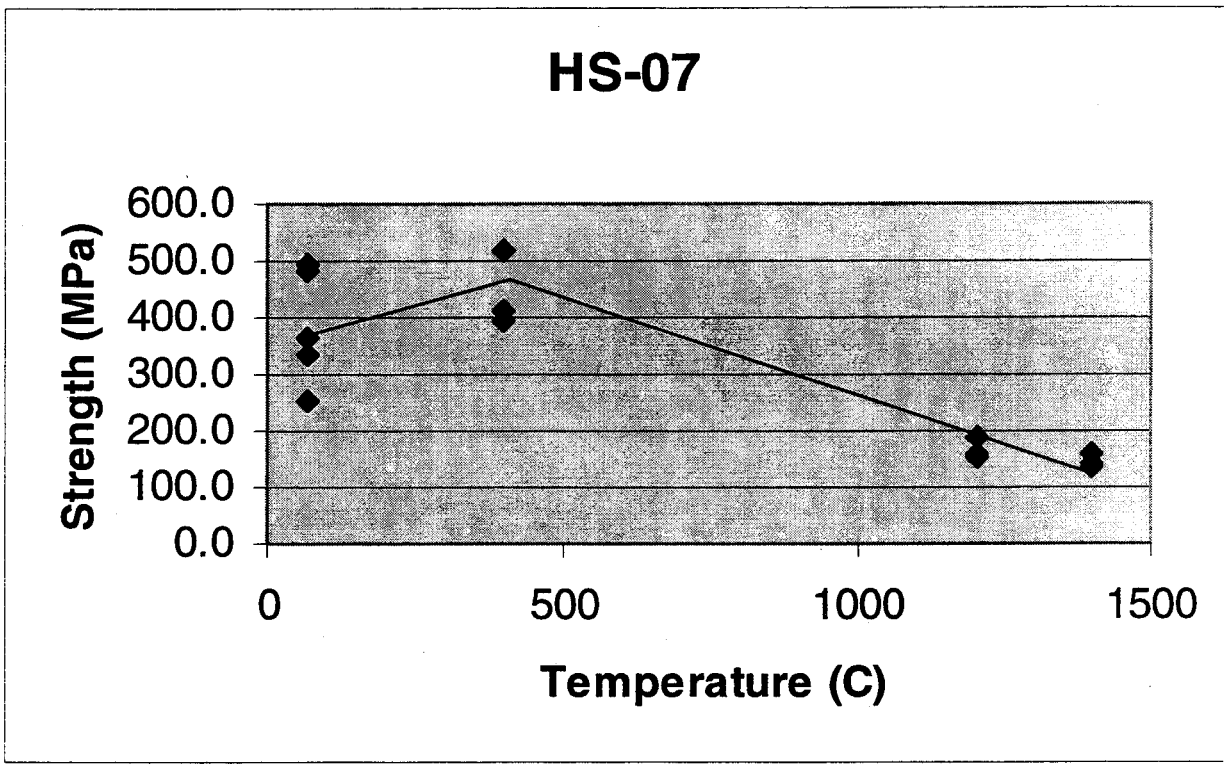

Figure 9 – Strength OF Flexure Bars As A Function of Temperature (HS-07).

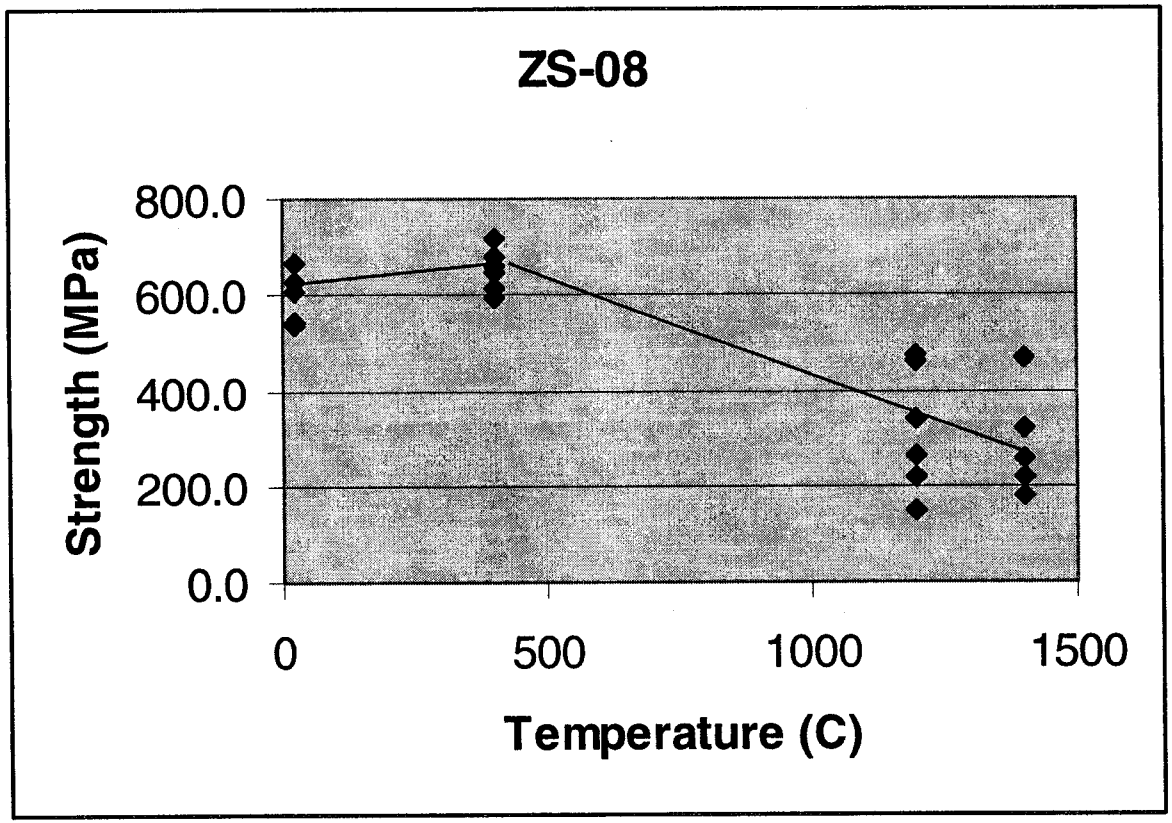

Figure 10 – Strength of Flexure Bars As A Function of Temperature.

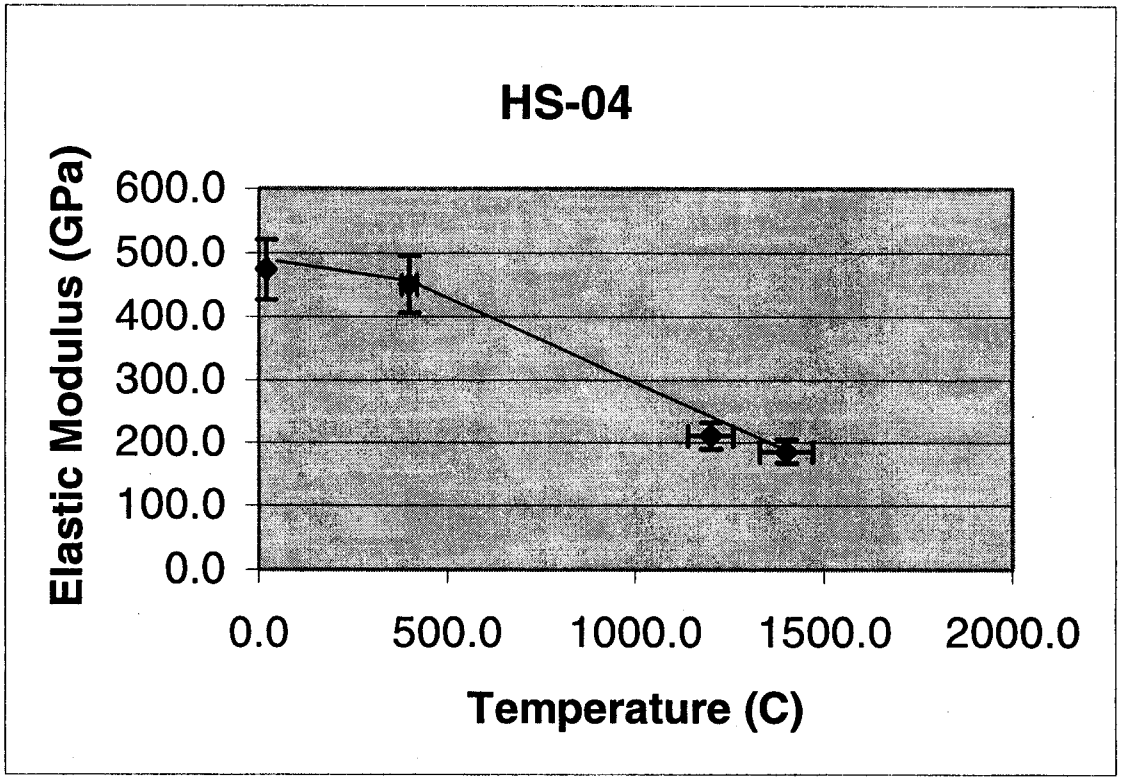

Figure 11 – Elastic Modulus As A Function of Temperature.

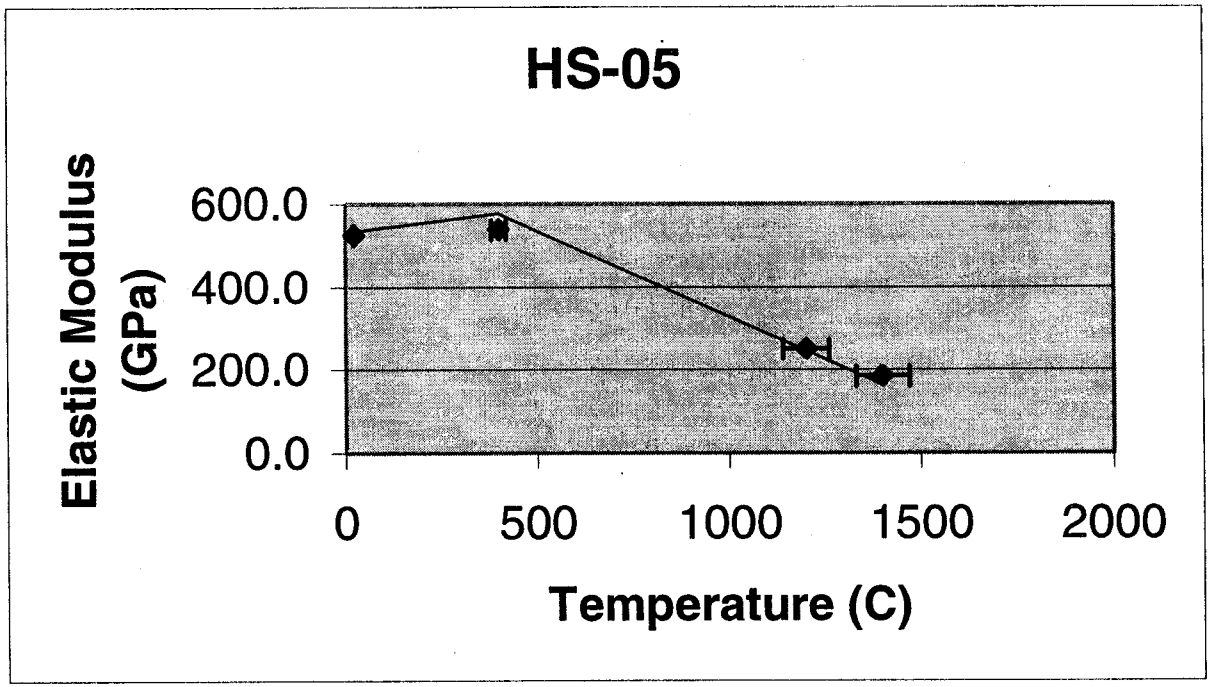

Figure 12 – Elastic Modulus Versus Temperature.

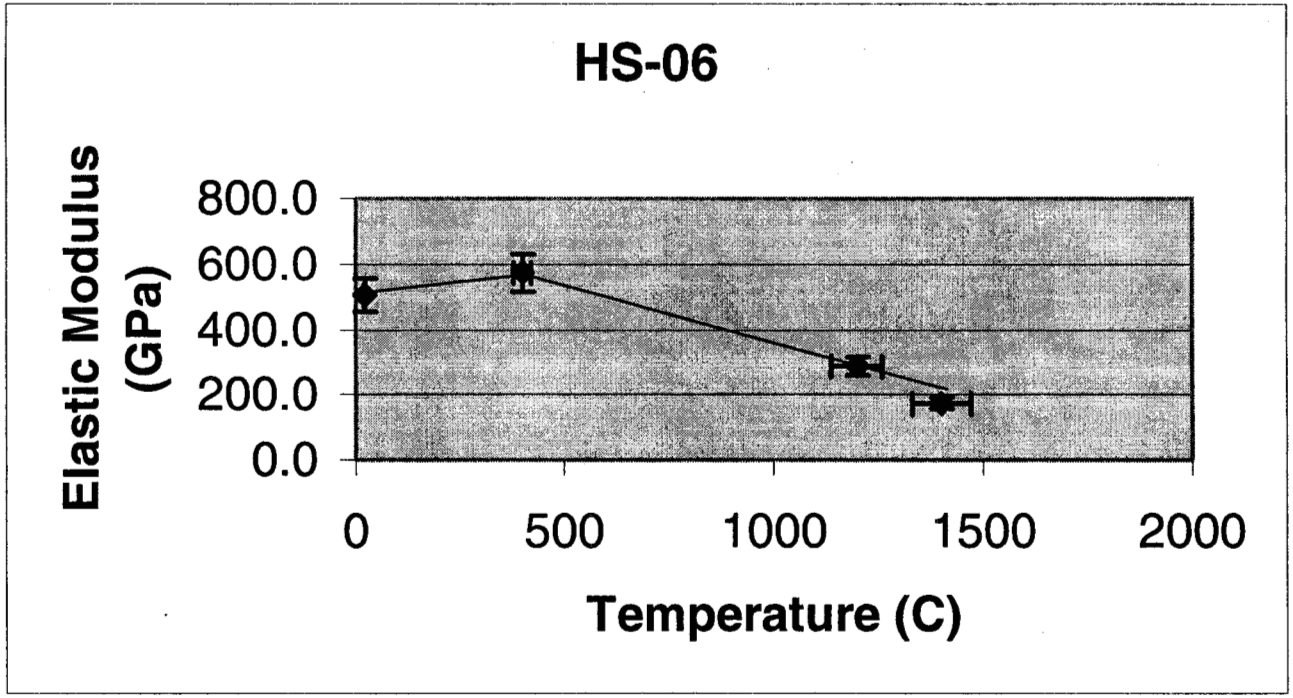

Figure 13 – Elastic Modulus As A Function of Temperature.

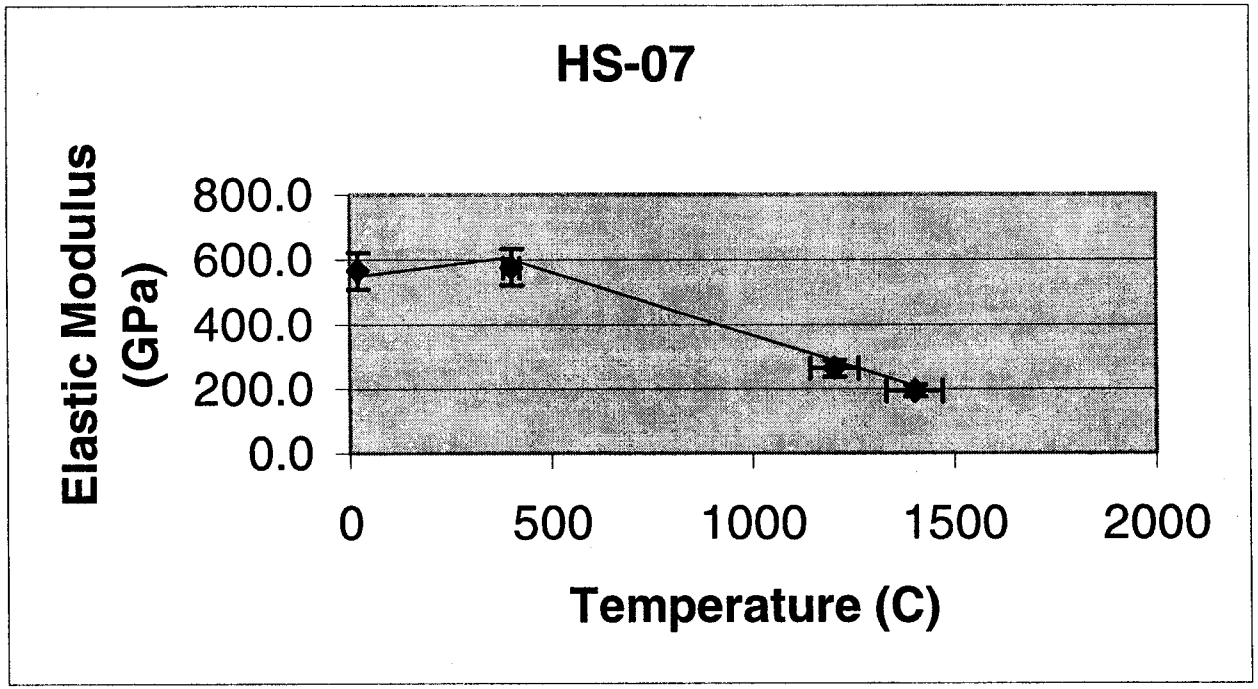

Figure 14 – Elastic Modulus As A Function of Temperature.

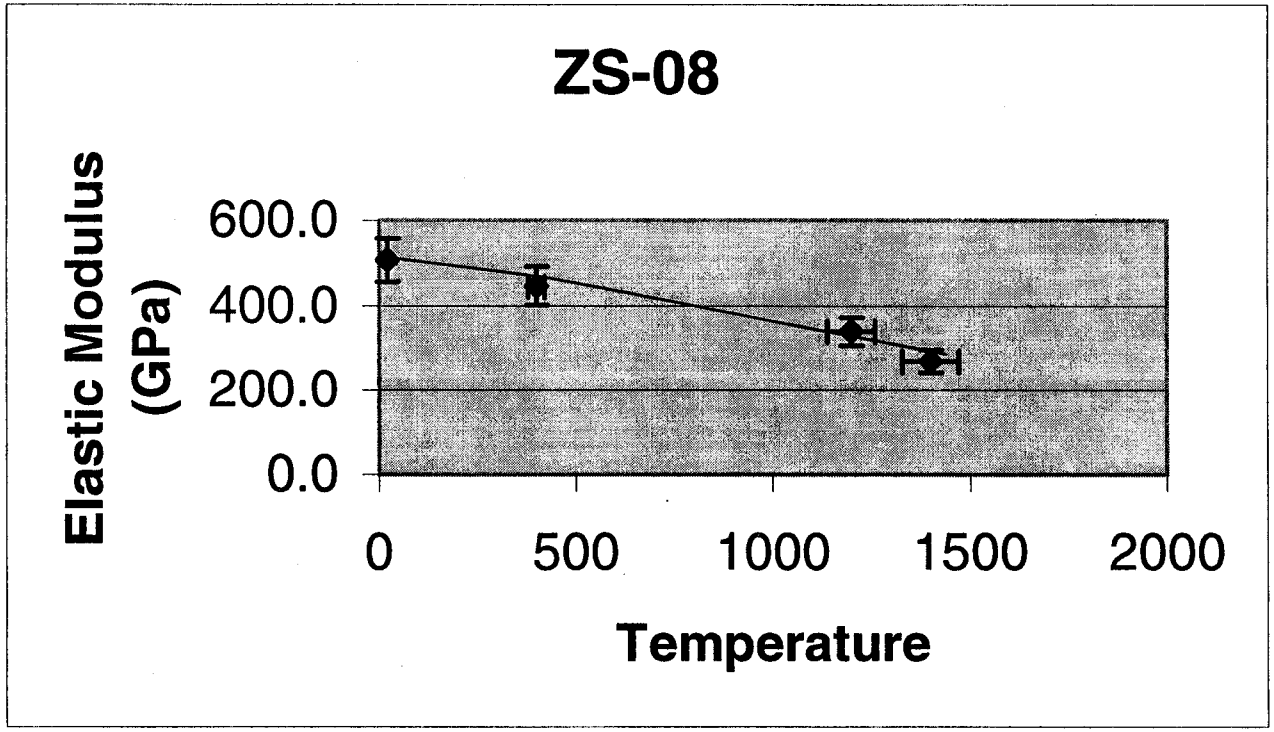

Figure 15 – Elastic Modulus As A Function of Temperature.

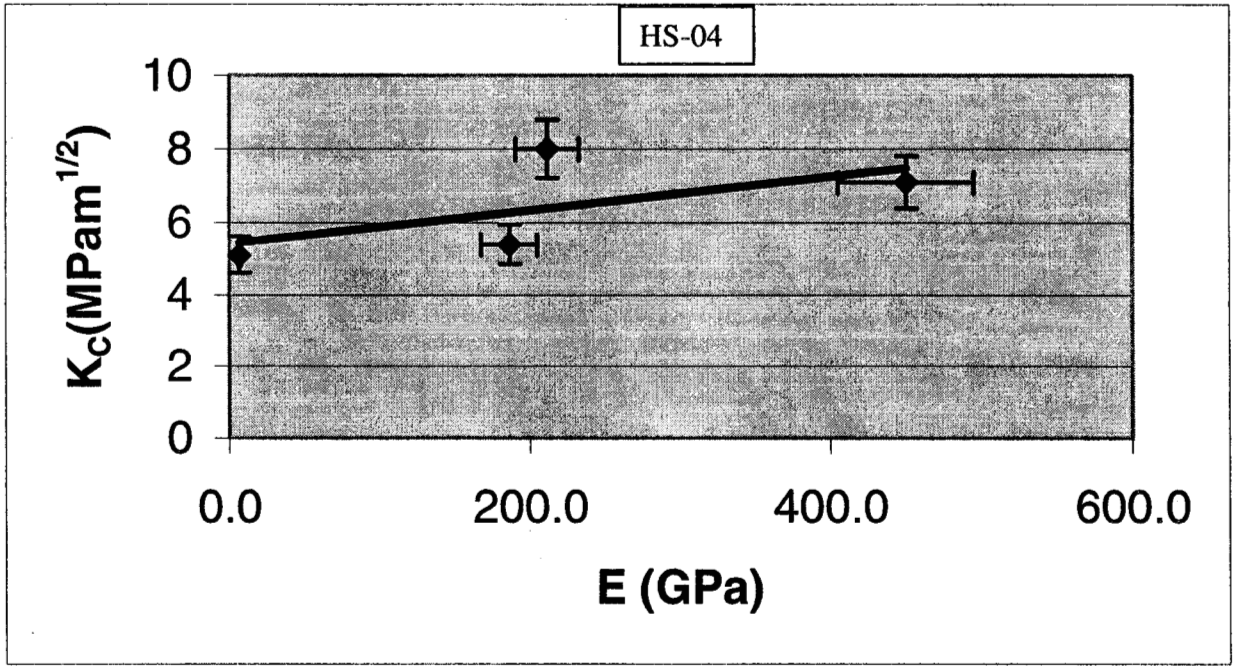

Figure 16 – Fracture Toughness (K_C) As A Function of Elastic Modulus (E) For HS-04.

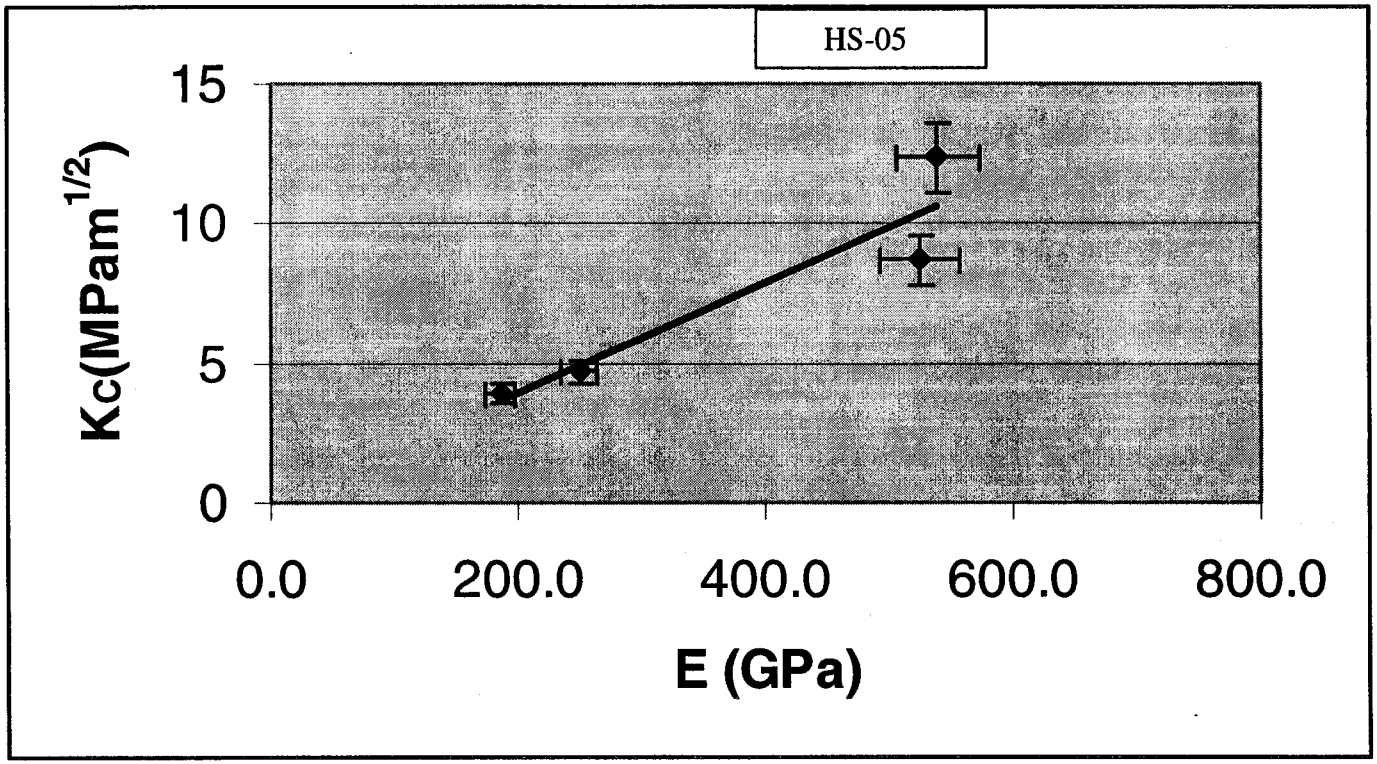

Figure 17 – Fracture Toughness (K_C) As A Function of Elastic Modulus (E) for HS-05.

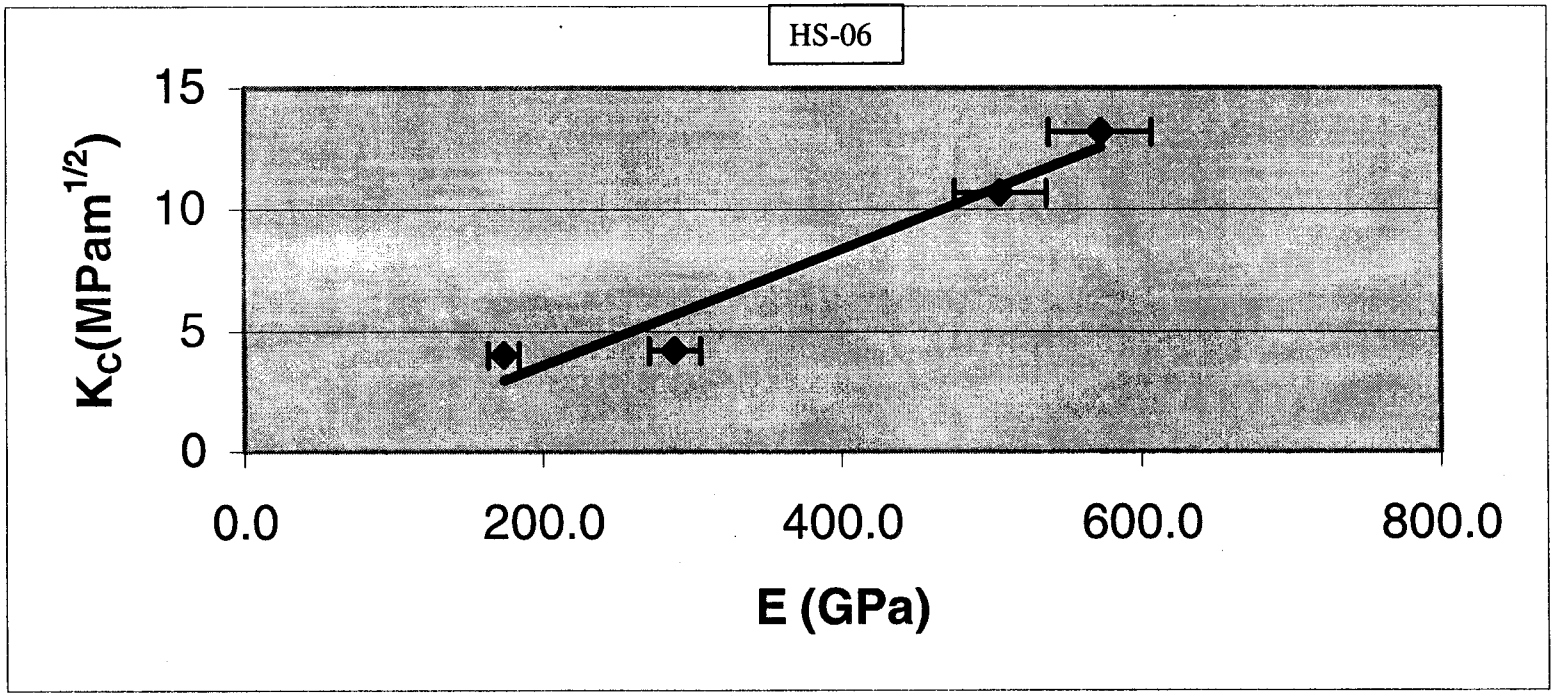

Figure 18 – Toughness (K_C) Versus Elastic Modulus (E) for HS-06.

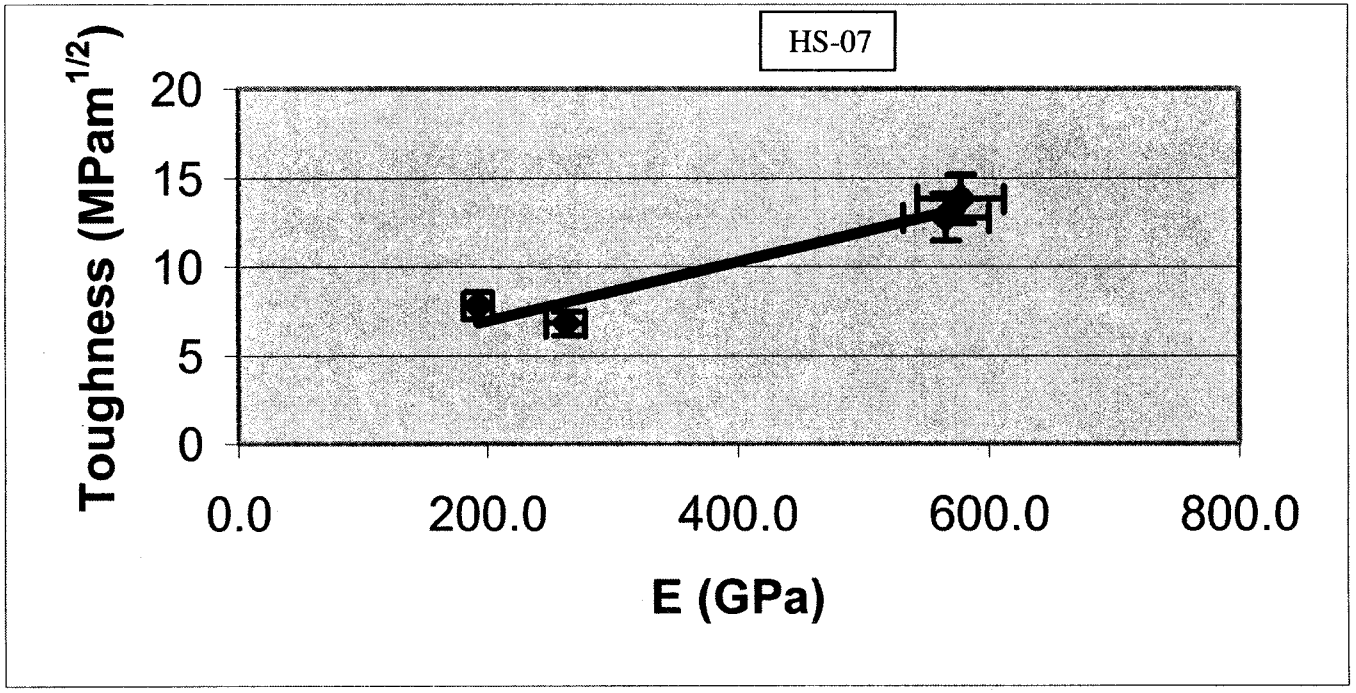

Figure 19 – Toughness As A Function of Elastic Modulus for HS-07.

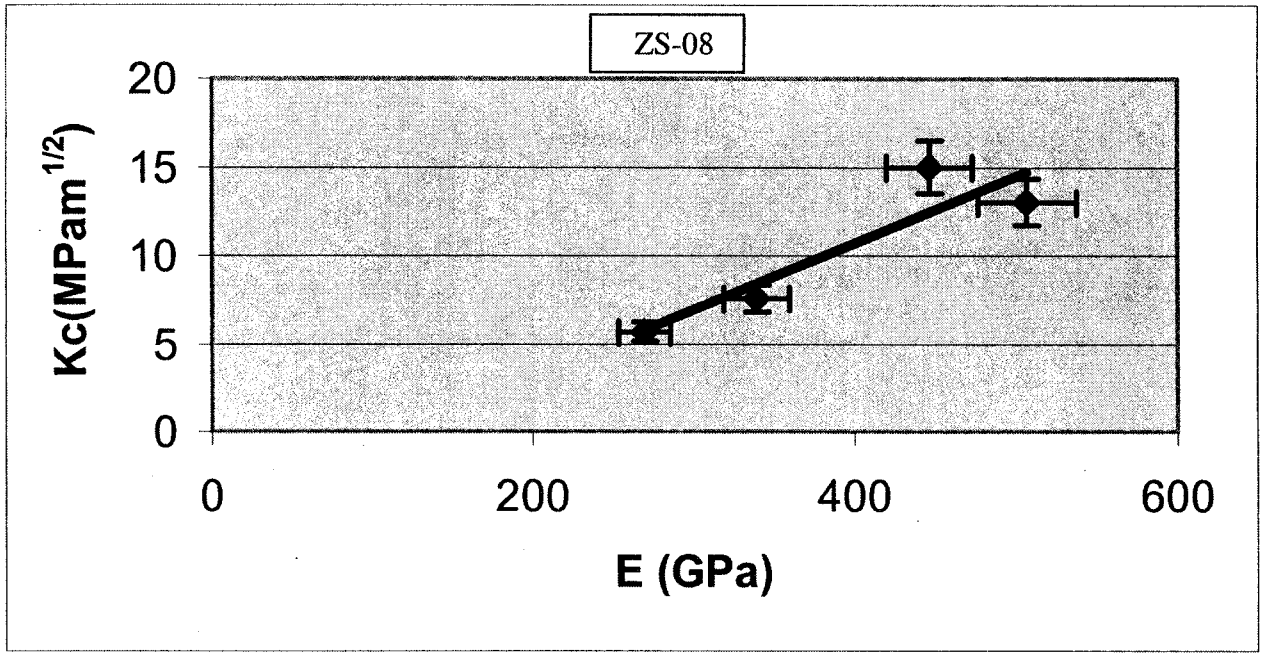

Figure 20 – Fracture Toughness (K_C) As A Function of Elastic Modulus (E) for ZS-08.
Solid line is a best fit line.

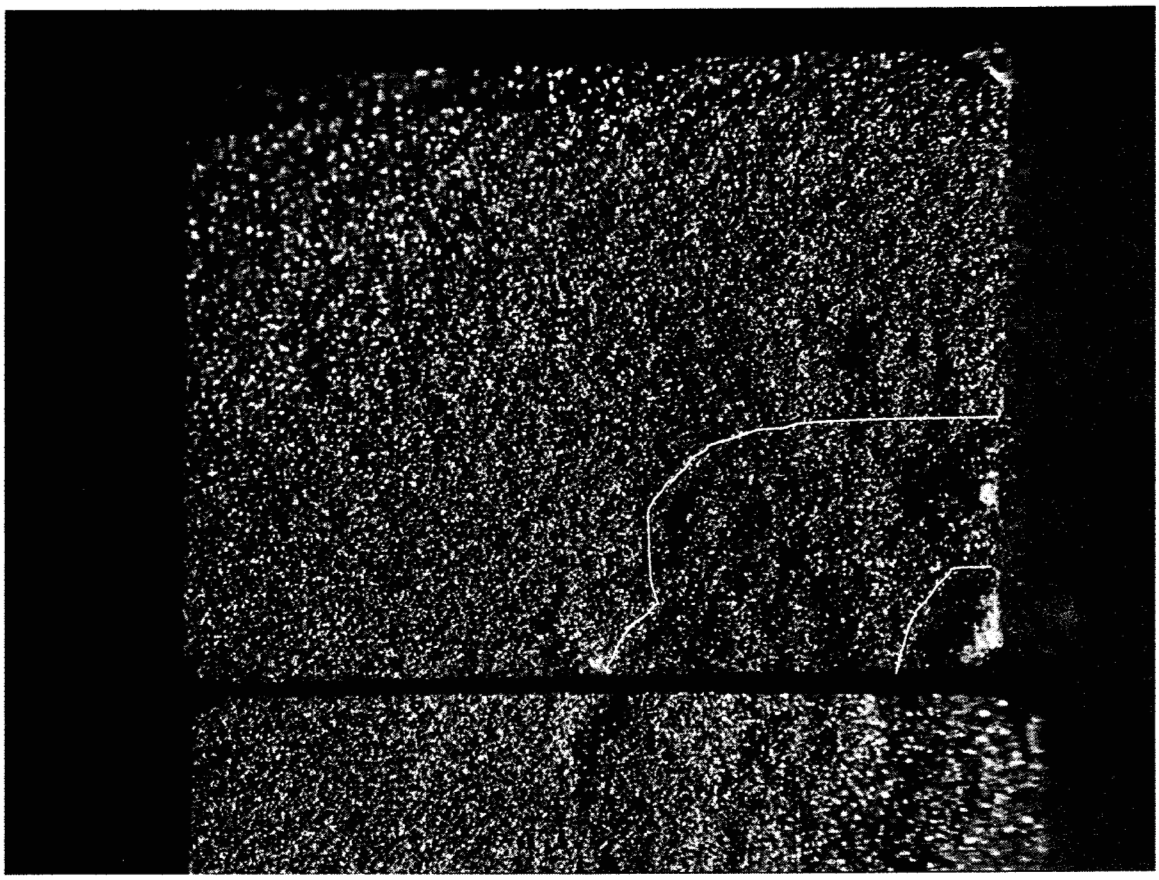

Figure 21 – Photograph of Fracture Surfaces of HS-05 (#16) Failed at 1400°C. Notice region of slow crack growth (larger line outlined inn white) and the original crack (smaller white line). Portion of matching half is in lower part of figure.[134MPa]

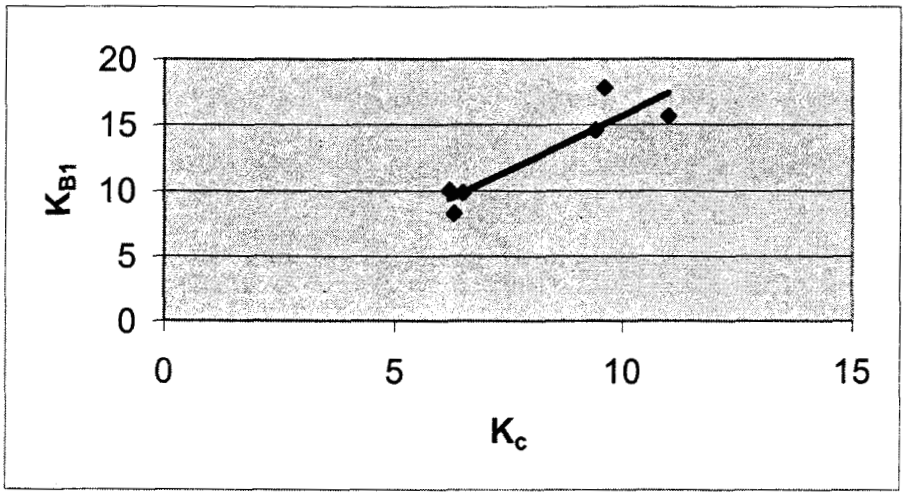

Figure 22 - Crack Branching Constant (K_{B1}) As A Function of Toughness (K_C) For All Materials.

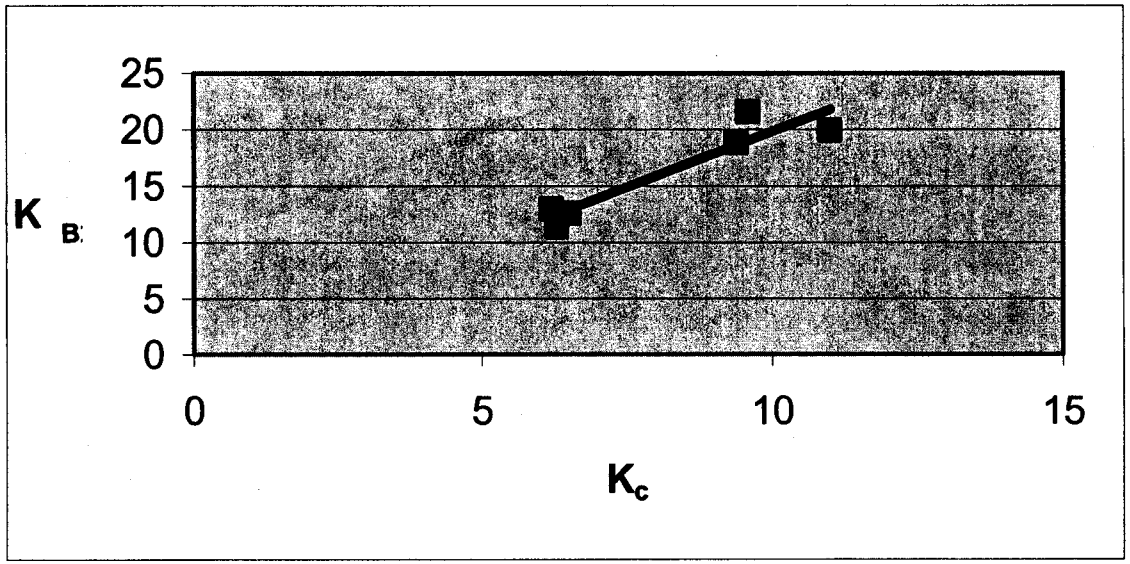

Figure 23 - Crack Branching Constant (K_{B2}) Is A Function of Toughness (K_C) For All Materials.

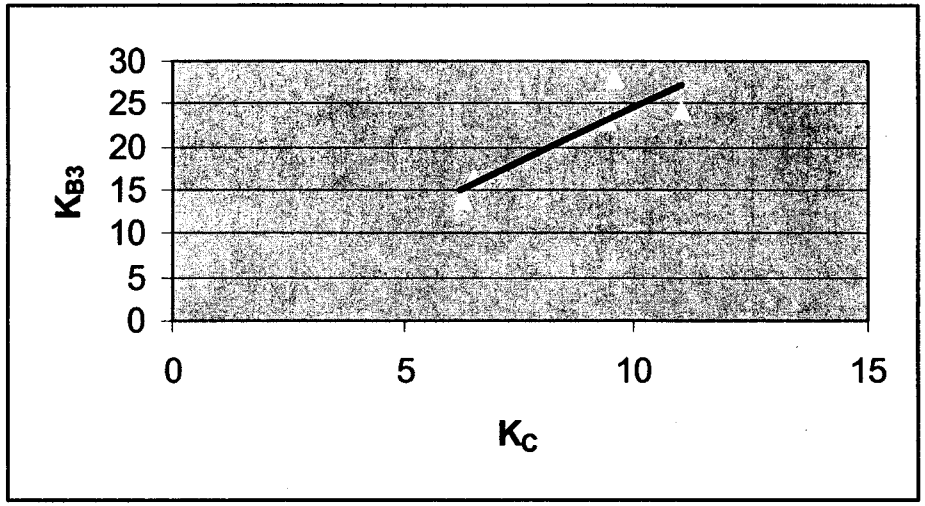

Figure 24 - Crack Branching Constant (K_{B3}) Is A Function of Toughness (K_C) For All Materials.

Appendix 1 - HS-04										
Orientation	Specimen	Temp.°C	Strength		Modulus		a	2b	c	K_C
		(°F)	(ksi)	MPa	(Mpsi)	GPa	m 10^{-6}	m 10^{-6}	m 10^{-6}	(MPam$^{1/2}$)
longitudinal	1	21°C	38.4	264.8	67.3	464.0	940	1400	810	9.3
HS04	5	(70°F)	37.5	258.6	65.3	450.2	320	1700	520	7.3
	9		33	227.5	56.9	392.3	500	850	480	6.2
	13		41.5	286.1	75.9	523.3	260	910	340	6.5
	17		39.2	270.3	78.3	539.9	240	1000	350	6.3
avg			**37.9**	261.5	**68.7**	**474.0**				**7.1**
stdev			**3.1**	21.5	**8.6**	**59.4**				**1.3**
				6.9		6.9				
longitudinal	2	400°C	44.3	305.4	66.1	455.8	300	1400	470	8.2
	6	(752°F)	40	275.8	63	434.4	440	490	470	8.4
	10		47.3	326.1	67.3	464.0	460	1200	530	9.3
	14		38.3	264.1	64.9	447.5	340	590	320	5.9
avg			**42.5**	292.9	**65.3**	**450.4**				**8.0**
stdev			**4.1**	28.2	**1.8**	**12.6**				**1.4**
				6.9		6.9				
longitudinal	3	1200°C	19.9	137.2	31.5	217.2	1200	2100	1100	5.6
	7	(2192°F)	10.9	75.2	28.7	197.9				
	11		16.7	115.1	28.1	193.7	900	3100	2100	4.9
	15		18.2	125.5	34.2	235.8	1.6	2.2	1300	5.6
avg			**16.4**	113.3	**30.6**	**211.2**				**5.4**
stdev			**3.9**	26.9	**2.8**	**19.4**				**0.4**
				6.9		6.9				
longitudinal	4	1400°C	19.6	135.1	26.1	180.0				
	8	(2552°F)	21.4	147.6	28.4	195.8	1000	1900	980	5.7
	12		19	131.0	27.6	190.3				
	16		18.7	128.9	21.5	148.2	1500	2000	1200	5.5
	18		21.8	150.3	31.4	216.5	500	960	490	4.1
avg			**20.1**	138.6	**27.0**	**186.2**				**5.1**
stdev			**1.4**	9.8	**3.6**	**25.0**				**0.9**

Appendix 2 - HS05										
Orientation	**Specimen**	**Temp °C**	**Strength**	**Strength**	**Modulus**	**E**	a	2b	c	K_{IC}
		(°F)	(ksi)	(MPa)	(Mpsi)	(GPa)	m 10^{6}	m 10^{6}	m 10^{6}	(MPam$^{1/2}$)
longitudinal	1	21	56.9	392.3	71.6	493.7				
HS05	5	(70°F)	50	344.8	79.8	550.2	400	1500	550	10
	9		53.2	366.8	77.5	534.4				
	13		62.6	431.6	82.9	571.6	330	600	310	9.4
	17		42	289.6	69.5	479.2	130	350	150	4.4
avg			**52.9**	365.0	**76.3**	525.8				**7.9**
stdev			**7.7**	53.1	**5.6**	38.6				3.1
longitudinal	2	400	62.1	428.2	72.1	497.1				
	6	(752°F)	57.8	398.5	82.9	571.6	1700	4400	1900	21.5
	10		58	399.9	79.8	550.2	360	930	410	10
	14		71.2	490.9	78.3	539.9	470	1150	520	13.9
avg			**62.3**	429.4	**78.3**	539.7				**15.1**
stdev			**6.3**	43.2	**4.5**	31.3				5.8
longitudinal	3	1200	24	165.5	34	234.4				
	7	(2192°F)	25	172.4	35.3	243.4	790	2300	950	6.6
	11		24.1	166.2	39.9	275.1	400	840	410	4.2
	15		20	137.9	35.7	246.2	390	600	340	3.2
avg			**23.3**	160.5	**36.2**	249.8				**4.7**
stdev			**2.2**	15.4	**2.6**	17.6				1.7
longitudinal	4	1400	19.7	135.8	29.3	202.0				
	8	(2552°F)	18	124.1	27.8	191.7	660	2600	920	4.7
	12		18.9	130.3	23.9	164.8				
	16		19.4	133.8	25.4	175.1	460	1190	520	3.8
	18		20.9	144.1	28	193.1	560	720	640c	3.2
avg			**19.4**	133.6	**26.9**	185.3				**3.9**
stdev			**1.1**	7.4	**2.2**	15.0				0.4

Appendix 3 - HS 06											
Orientation	**Specimen**	**Temp °C**	**Strength**	**Strength**	**Modulus**	**E**	**a**	**2b**	**c**	**Y**	K_{IC}
		(°F)	**(ksi)**	**MPa**	**(Mpsi)**	**GPa**	**m10^6**	**m10^6**	**m 10^6**		**(MPam$^{1/2}$)**
longitudina	2	21	41.2	284.1	74.8	515.7	550	1300	600	1.24	8.6
HS 06	6	(70°F)	50.3	346.8	79.5	548.2					
	10		39.3	271.0	71.6	493.7	880	2700	1100	1.24	11.1
	14		43.5	299.9	70.2	484.0	810	2300	970	1.24	11.6
	18		50	344.8	70.9	488.9	680	1300	660	1.24	11
avg			**44.9**	309.3	**73.4**	506.1					**10.6**
stdev			**5**	34.8	**3.8**	26.5					1.3
						6.9					
longitudina	3	400	59.6	410.9	84.5	582.6	510	1200	550	1.24	12
	7	(752°F)	65.7	453.0	85.5	589.5	450	2200	703	1.24	14.9
	11		55.3	381.3	78.7	542.6					
	15		65.4	450.9	83.8	577.8	550	1000	520	1.24	12.8
avg			**61.5**	424.0	**83.1**	573.1					**13.2**
stdev			**5.0**	34.5	**3.0**	20.9					1.5
						6.9					
longitudina	4	1200	20.6	142.0	41	282.7	740	1300	700	1.24	3.8
	8	(2192°F)	21.4	147.6	49.4	340.6	360	1150	640	1.24	4.6
	12		19.3	133.1	36.3	250.3	660	1800	770	1.24	4.6
	16		18.5	127.6	40.4	278.6	380	1100	460	1.24	3.4
avg			**20.0**	137.6	**41.8**	288.0					**4.1**
stdev			**1.3**	8.9	**5.5**	37.9					0.6
						6.9					
longitudina	1	1400	17.5	120.7	29.5	203.4	820	1200	700	1.24	3.2
	5	(2552°F)	15.4	106.2	21.3	146.9	630	1200	615		3.3
	9		16.7	115.1	23.8	164.1					
	13		15.9	109.6	22.8	157.2	1400	2200	1200		4.7
	17		17.5	120.7	28.7	197.9	910	2200	1000		4.7
avg			**16.6**	114.5	**25.2**	173.9					**4.0**
stdev			**0.9**	6.5	**3.7**	25.3					0.8

Appendix 4 - HS-07											
Orientation	Specimen	Temp (°C)	Strength	Strength	Modulus	E	a	2b	c	Y	K_c
		(°F)	(ksi)	(MPa)	(Mpsi)	(GPa)	$m10^6$	$m10^6$	$m10^6$		($MPam^{1/2}$)
longitudinal	1	21	53.3	367.5	78.6	541.9					
HS07	3	(70°F)	70	482.7	83.8	577.8	343	1810	557	1.24	14.1
	7		37	255.1	78.6	541.9					
	11		48.8	336.5	83.5	575.7	606	956	538	1.24	9.7
	15		71.7	494.4	85.8	591.6	482	1343	568	1.24	14.6
avg			**56.2**	387.2	**82.1**	565.8					**12.8**
stdev			**14.7**	**101.2**	**3.3**	**22.6**					2.7
longitudinal	4	400	75.4	519.9	84.5	582.6					
	8	(752°F)	57.1	393.7	86.2	594.3	754	2406	952	1.24	15.1
	12		56.8	391.6	85.5	589.5	732	1774	806	1.24	13.8
	16		59.7	411.6	78.9	544.0	510	1409	600	1.24	12.5
avg			**62.3**	**429.2**	**83.8**	**577.6**					**13.8**
stdev			**8.9**	61.1	**3.3**	22.9					1.3
longitudinal	5	1200	27.2	187.5	40.7	280.6	1641	2051	1835	1.4	11.2
	9	(2192°F)	21.9	151.0	37	255.1	610	3392	1017	1.24	6
	13		23.3	160.7	39.3	271.0	760	1197	674	1.24	5.2
	17		21.9	151.0	35.7	246.2	452	1630	607	1.24	4.6
avg			**23.6**	**162.5**	**38.2**	**263.2**					**6.8**
stdev			**2.5**	17.3	**2.2**	15.5					3.0
longitudinal	2	1400	23	158.6	28.7	197.9	1277	1672	1461	1.4	8.5
	6	(2552°F)	20.1	138.6	25.8	177.9	1328	2263	1733	1.4	8.1
	10		20.4	140.7	25.8	177.9	1416	1898	1639	1.4	8
	14		20.1	138.6	25.5	175.8	1109	1971	1478	1.4	7.5
	18		19.4	133.8	34	234.4	1044	1898	1408	1.4	7
avg			**20.6**	**142.0**	**28.0**	**192.8**					**7.8**
stdev			**1.4**	9.6	**3.6**	25.0					0.6

Appendix 5 - ZS-08										
Orientation	Specimen	Temp °C	Strength	Strength	Modulus	E	a	2b	c	K_{IC}
		(°F)	(ksi)	(MPa)	(Mpsi)	(GPa)	$m10^6$	$m10^6$	$m10^6$	($MPam^{1/2}$)
longitudinal	1	21	79	544.7	70.3	485.0	220	350	200	9.6
ZS08	5	(70°F)	90.8	626.1	78.1	538.7	350	940	400	15.5
	9		88	606.8	70.2	484.3	390	1000	450	16
	13		77.6	535.1	69.6	480.1	350	440	280	11
	17		96.6	666.1	79.3	546.4				
avg			**86.4**	595.7	**73.5**	506.9				**13.0**
stdev			**8.0**	55.4	**4.7**	32.7				3.2
longitudinal	2	400	93.9	647.4	64.7	446.2				
	6	(752°F)	95.4	657.8	66.5	458.5			300c	15.9
	10		103.6	714.3	67.4	465.0	300	830	350	16.6
	14		89.4	616.4	64.9	447.5	350	460	280	12.9
	18		86.2	594.3	61.1	421.4	310	600	310	13.1
	21		98.2	677.1	63.8	439.6				
avg			**94.5**	651.2	**64.7**	446.3				**14.6**
stdev			**6.2**	42.8	**2.2**	15.3				1.9
				6.9						
	3				49.7	342.4	370	540	320	7.5
longitudinal	3	1200	49.2	339.2	49.8	343.2	370	540	450c	10
	7	(2192°F)	31.9	220.0	51.8	357.3				
	11		66.4	457.8	44.4	306.3	290	500	270	9.3
	15		21	144.8	46.3	319.3	600	990	550	4.2
	19		68.9	475.1	53.3	367.6				
	22		37.9	261.3	**49.2**	339.3	550	700	470	7.1
avg			**46**	316.4	**3.3**	23.0				**7.6**
stdev			**19**	132.3						2.6
					35.4	244.4				
longitudinal	4	1400	46.3	319.2	33.5	230.8	230	500	240	6.1
	8	(2552°F)	36.9	254.4	45.5	313.8	500	730	430	6.5
	12		67.9	468.2	36.9	254.4				
	16		26	179.3	44.4	306.3	380	960	430	4.6
	18		31.8	219.3	**39.1**	269.9				
avg			**41.8**	288.1	**5.5**	37.7				**5.7**
stdev			**16.4**	113.0						1.0

Distribution :

MS-1174 A. Hodapp, 15414
MS-1174 D. Keese, 15414
MS-1411 S. J. Glass, 1843
MS-1411 S. Monroe, 1843
MS-1411 E. Beauchamp, 1843
MS-1349 R. Loehman, 1843
MS-0887 A. K. Hays, 1800
MS-0188 LDRD Office (5)
MS-9018 Central Technical Files, 8945-1
MS-0899 Technical Library 9616
MS-0612 Review and Approval Desk, 9612

Dr. Sylvia Johnson
NASA Ames Research Center
MS 234
Moffett Field, CA 94035

Dr. Don Ellerby
NASA Ames Research Center
MS 234-1
Moffett Field, CA 94035

Dr. Jon Salen
NASA Glenn Space Center
21000 Brookpark Rd.
Cleveland, OH 44135